Settling fluxes and sediment accumulation rates by the combined use of sediment traps and sediment cores in Tema Harbour (Ghana)

Benjamin O. Botwe [a,d,*], José M. Abril [b], Antonio Schirone [c], Mattia Barsanti [c], Ivana Delbono [c], Roberta Delfanti [c], Elvis Nyarko [d], Piet N.L. Lens [a]

[a] IHE-DELFT Institute for Water Education, PO Box 3015, 2601 DA Delft, The Netherlands
[b] Departamento de Física Aplicada I, ETSIA Universidad de Sevilla, Carretera de Utrera km 1, D.P., 41013 Seville, Spain
[c] ENEA, Marine Environment Research Centre, P.O. Box 224, I-19100 La Spezia, Italy
[d] University of Ghana, Department of Marine and Fisheries Sciences, PO Box LG 99, Legon, Accra, Ghana

HIGHLIGHTS

- Sediment traps deployed and sediment cores collected in Tema Harbour for the first time.
- A multi-tracer approach with Gamma spectrometry is applied in a disturbed harbour area.
- TERESA model is a good tool in disturbed sites where common ^{210}Pb dating models fail.
- TERESA model sediment accumulation rates in Tema Harbour are 1.4–3.0 g·cm^{-2}·y^{-1}.

GRAPHICAL ABSTRACT
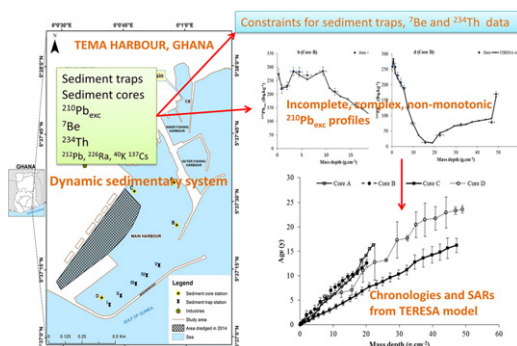
ABSTRACT

Settling fluxes and sediment accumulation rates in coastal Tema Harbour (Ghana) were investigated by the com-bined analyses of results in sediment traps and sediment cores. Sediment traps were deployed at 5 stations with-in the Tema Harbour at two sampling depths and were retrieved every two weeks till the end of 12 weeks to estimate the Settling Fluxes (SFs). Four sediment cores from the harbour were analysed for their radioactivity (^{7}Be, ^{234}Th, ^{210}Pb, ^{212}Pb, ^{226}Ra, ^{40}K and ^{137}Cs) profiles to quantify Sediment Accumulation Rates (SARs). The sed-iment cores exhibited variable bulk density profiles, indicating highly dynamic and non-steady sedimentation conditions. ^{7}Be-derived gross-estimates of very recent SARs using the constant flux-constant sedimentation (CF-CS) model were in the range of 2.5–9.0 g·cm^{-2}·y^{-1}. These values were much lower than the estimated aver-age SFs (15.2–53.8 g·cm^{-2}·y^{-1}), indicating sediment resuspension plays an important role. On a decadal time scale, conventional ^{210}Pb sediment dating models did not allow any estimation of SARs in the Tema Harbour. Thus, the ^{210}Pb-based TERESA model was applied to depict a reliable scenario for sedimentation with time-averaged SARs in the range of 1.4–3.0 g·cm^{-2}·y^{-1} and fluxes of matter contributed by the marine inflow and local sources. Sediment accretion rates of 1.7–3 cm·y^{-1} were also inferred, which may pose a moderate problem of sustainability for the Tema Harbour. This study reveals how the geochemical behaviour of different radionuclides with Gamma spectrometry in the marine environment can be used to obtain reliable information on the complex dynamics of Suspended Particulate Matter (SPM), even in a very disturbed and anthropic environment as a coastal harbour area where (1) conventional 210Pb-based dating methods fail and (2) the use of sediment traps and 234Th and 7Be profiles in sediment cores show serious constraints.

* Corresponding author at: IHE-DELFT Institute for Water Education, PO Box 3015, 2601 DA Delft, The Netherlands.
  E-mail address: bbotwe@ug.edu.gh (B.O. Botwe).

1. Introduction

Coastal marine harbours support national economies through shipping, fishing and tourism and are, therefore, considered important assets for coastal nations (Van Rijn, 2005). Coastal marine harbours are prone to large influxes of sediments as a result of waves and tidal currents (Leys and Mulligan, 2011), as well as erosion downdrift of the harbour breakwater. In semi-enclosed coastal harbours, the restricted water movement may enhance the settling of sediments and result in their accumulation within the harbour basin (Lepland et al., 2010; Botwe et al., 2017a). Sediment accumulation in harbours poses navigation and ecological challenges (Syvitski et al., 2005; Van Rijn, 2005; Green and Coco, 2014), requiring dredging at high costs (Qu and Kelderman, 2001; Barneveld and Hugtenburg, 2008; Schipper et al., 2010). Human activities around harbours often result in the accumulation of a variety of hazardous pollutants in sediments (Botwe et al., 2017a, 2017b), which poses serious concerns about the handling and fate of the dredged materials. Sedimentation in harbours is thus a major issue and its quantification is essential for harbour management (Buesseler et al., 2007; Leys and Mulligan, 2011).

Information on sediment accumulation rates (SARs) in harbours, reservoirs, estuaries and coastal areas can be obtained from the comparison of bathymetric data acquired at different periods (Khaba and Griffiths, 2017, Brucker et al., 2007). This GIS-bathymetric approach involves measurements of tidal levels, water depth, positioning and the application of a series of corrections. For shallow waters with <20 m water depth such as harbours, bathymetric data can be best obtained by using Phase Differencing Bathymetric Sonar (PDBS) systems with an associated total vertical uncertainty of 0.26 m for a 10 m water depth (Brisson et al., 2014). Although this uncertainty is acceptable for water depth control purposes, it is too coarse for estimating SARs. Thus, GIS-bathymetry has been mainly used for mapping SAR in areas where accretion rates are high (>0.3 m·y^{-1}) (Brucker et al., 2007) or when the study involves time lapses of the order of decades (Ortt et al., 2000). It is worth noting that the method provides mean SAR in the time lapse and it cannot identify processes affecting the depth distribution of hazardous pollutants. Other methods based on horizon markers, anchored tiles, rulers, sediment traps, optical backscatter sensors and short-lived radionuclides (^{234}Th and ^{7}Be) are available for measuring sediment accumulation over short-time scales (Thomas and Ridd, 2014).

In depositional environments, where continuous accumulation of sediments has taken place over a long period of time without any interruption in the sedimentary sequence or mixing, the ^{210}Pb sediment dating technique has proven useful for quantifying SARs on time scales spanning 100–150ssears (Appleby and Oldfield, 1978; Robbins, 1978; Appleby and Oldfield, 1983; Caroll and Lerche, 2003; Alonso-Hernandez et al., 2006; Díaz-Asencio et al., 2011; Bellucci et al., 2012). Sedimentation in coastal marine harbours is, however, a dynamic process for which relatively large spatial and temporal variations can be expected (Leys and Mulligan, 2011). For example, sediment resuspension due to wave action, tidal oscillations, movement of vessels and dredging (Lepland et al., 2010; Leys and Mulligan, 2011; Green and Coco, 2014) may co-occur with sediment deposition in coastal marine harbours. Thus, complete recovery of radionuclide inventories could also be difficult in areas with relatively high SARs (of the order of 1 g·cm^{-2}·y^{-1}) due to the limited length of sediment core samplers. Quantifying sedimentation rates in such disturbed environments, therefore, requires integrated approaches (Bellucci et al., 2012), the application of robust numerical models and an accurate study of the harbour and the operations within the harbour itself (Tanner et al., 2000; Tang et al., 2008; Smith et al., 2009; Lepland et al., 2010).

As far as we know, there are no previous studies on harbours located in tropical Africa, where in addition to the aforementioned challenges and the scarcity of background studies, it is difficult to measure artificial radionuclides such as ^{137}Cs above the method detection limit due to its low fallout rate. ^{210}Pb-based chronologies require independent chronostratigraphic markers for validation (Smith, 2001; Caroll and Lerche, 2003; Abril, 2004) and ^{137}Cs is the most widely used complement for the ^{210}Pb dating method.

Profiles of short-lived and particle-reactive radionuclides such as ^{234}Th (half-life = 24 d) and ^{7}Be (half-life = 53 d) in sediment cores can be used to estimate recent sedimentation rates over short-time scales of days to months (Giffin and Corbett, 2003). ^{234}Th is produced from the decay of ^{238}U (half-life = 4.5×10^9 y), while ^{7}Be is a cosmogenic radionuclide produced from the interaction of cosmic rays with oxygen and nitrogen in the stratosphere and the troposphere (Sharma et al., 1987; Erten, 1997; Pfitzner et al., 2004; Palinkas et al., 2005). In marine environments, ^{238}U is found in the water column in excess with respect to ^{226}Ra due to its higher solubility (IAEA, 2004; Botwe et al., 2017b). When ^{238}U decays to ^{234}Th, this high particle-reactive isotope is taken up by Suspended Particulate Matter (SPM) and surface sediments, where it can be found in excess with respect to the background levels, referred to as excess ^{234}Th (^{234}Th$_{exc}$). ^{7}Be and ^{234}Th$_{exc}$ profiles, when combined with ^{210}Pb and ^{137}Cs profiles in sediment cores, are useful for understanding sediment dynamics in aquatic systems (Sharma et al., 1987; Erten, 1997; Fuller et al., 1999; Giffin and Corbett, 2003; Palinkas et al., 2005; Yeager et al., 2005; Schmidt et al., 2007a; Schmidt et al., 2007b). In addition to radionuclide profiles in sediment cores, sediment traps are important tools for investigating short-term fluxes and dynamics of sediments in aquatic systems (Kelderman, 2012; Kelderman et al., 2012; de Vicente et al., 2010).

The objective of this study was to investigate settling fluxes and sedimentation rates in the coastal marine Tema Harbour (Ghana) by the combined analyses of accumulated dry mass in sediment traps and radionuclide (^{7}Be, ^{234}Th, ^{210}Pb, ^{212}Pb, ^{226}Ra, ^{40}K and ^{137}Cs) profiles in sediment cores, with the help of numerical sediment dating models. In particular, excess ^{210}Pb (^{210}Pb$_{exc}$) data were analysed with the TERESA (Time Estimates from Random Entries of Sediments and Activities) model (Abril, 2016), which is based on a widely observed statistical correlation between ^{210}Pb$_{exc}$ fluxes and SARs (Abril and Brunskill, 2014). The TERESA model has been validated against synthetic cores and real data from varved sediments, for which an independent chronology was available. The basic assumptions of the TERESA model were satisfied by the sedimentary conditions in the disturbed Tema Harbour, which provided a unique opportunity to test the performance of this new dating tool under conditions where the assumptions of most of the ^{210}Pb-based models fail. Thus, this study may be of interest to the broad scientific community concerned with the investigation of sedimentation conditions and pollution records in harbours and other dynamic systems where SAR values fall beyond the capabilities of the differencing GIS-bathymetry and conventional ^{210}Pb-based dating methods, and the use of sediment traps and ^{234}Th and ^{7}Be profiles show serious constraints.

2. Materials and methods

2.1. Study area

The Tema Harbour is about 70 km west from the outlet of the Volta River in Ghana and there are several minor riverine systems along the Ghanaian shoreline that deliver important loads of suspended particulate matter to the coastal region (Akrasi, 2011). However, there is no

direct riverine inflow in the Tema Harbour (Botwe et al., 2017b). The Tema Harbour layout and its operations have been described previously (Botwe et al., 2017a; Botwe et al., 2017b; Botwe et al., 2017c). Briefly, the Tema Harbour is a semi-enclosed coastal harbour situated in the Gulf of Guinea at Tema (Greater Accra, Ghana) with a water area of 1.7 km² (Fig. 1). It has been in operation since 1962 and is partitioned into a Main Harbour, a Fishing Harbour (Inner and Outer) and a Canoe Basin. The Main Harbour is concerned with shipping operations and has water depths ranging from 7.5 to 11.4 m (mean 8.5 m), a 240 m wide entrance and a breakwater of 4850 m length (Botwe et al., 2017b). The Fishing Harbour and the Canoe Basin are dedicated to the operations of semi-industrial, industrial and artisanal fishing vessels (Botwe et al., 2017c).

The average water temperature is around 23 °C with water salinity ranging from 30–35‰ (Botwe et al., 2017c). Tides in the study area are semi-diurnal with a tidal range of about 1.6 m. In the immediate coastal sea area, tidal currents range from <0.1 to 0.5 m·s⁻¹ and wave heights

range from 1 to 2 m (http://open_jicareport.jica.go.jp/pdf/11681632_03.pdf). A portion of the Main Harbour (shown in Fig. 1) was dredged in March–April 2014, while the Canoe Basin was dredged in May 2013 (Botwe et al., 2017c). It is also worth noting that in 2013, the construction of a new wharf was started near the eastern margin of the dredged area, with the emplacement of the supporting concrete pillars. The overwater structure was completed during 2014.

2.2. Sediment sampling

Four sediment cores were sampled with an Uwitech® gravity corer (length = 60 cm; internal diameter = 8.5 cm) from stations A, B, C and D in the Tema Harbour (Fig. 1) in April 2015. Water depths at the sediment core stations A, B, C and D were 8.5, 8, 10 and 9 m, respectively. During the sediment core sampling period, the turbidity of seawater was measured in Nephelometric Turbidity Unit (NTU) at the surface, mid
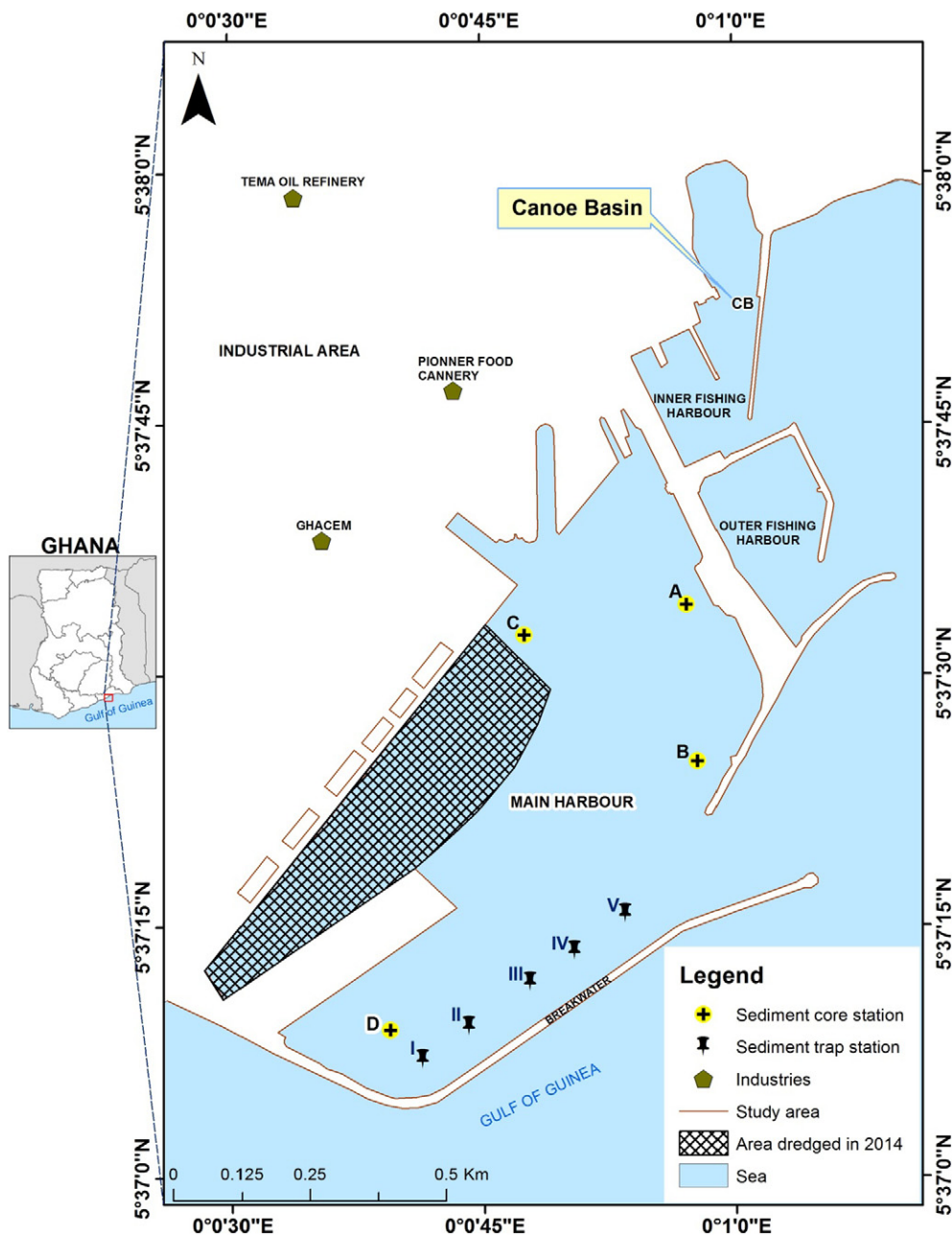

Fig. 1. Map of Tema Harbour (Ghana) showing sediment core and sediment trap sampling stations and the approximate area dredged in 2014.

depth and the bottom at each core sampling station using a turbidity probe (HI 9829, Hanna Instruments, USA).

Besides, vertical arrays of 2 cylindrical PVC sediment traps, positioned 0.6 m apart in an alternating fashion, were deployed at 5 stations (I, II, III, IV and V) along a transect in a less busy area of the Tema Harbour (Fig. 1) over a period of 12 weeks (23 May–15 August 2015) to collect settling particles at two water depths of approximately 1.8 m (top trap) and 0.6 m (bottom trap) from the seabed. The aspect ratio of each sediment trap was 6.0 (i.e. height = 60 cm; diameter = 10 cm) to minimise current-induced resuspension and loss of material from the trap (Bloesch and Burns, 1980; Kelderman et al., 2012; de Vicente et al., 2010). The sediment traps were retrieved every two weeks (Kelderman, 2012; Kelderman et al., 2012; de Vicente et al., 2010) till the end of the 12-week period. Upon their retrieval, the sediment cores and trap samples were placed upright in racks and transported to the Department of Marine and Fisheries Sciences laboratory at the University of Ghana for further processing and analysis. Rainfall data over the study period was obtained from the Ghana Meteorological Services.

In the laboratory, the sediment cores were allowed to stand overnight, after which the overlying water was carefully siphoned off. Each sediment core was sectioned at 1 cm intervals over the top 2 cm layer and subsequently at 2 cm intervals. During core extrusion and sectioning, lower sections may become contaminated as they move past smears from upper sections left on the walls of the corer. Thus, the outer 1 cm rim of each sediment slice was trimmed off (Bellucci et al., 2012). The content of each sediment trap was sieved successively over 2000 and 63 μm stainless steel mesh sieves to determine the distribution of the <63 μm (silt-clay) and 63–2000 μm (sand) fractions of the trapped sediment. The wet weights of the sediment core samples, the core layers, as well as the <2000 μm fraction of sediment trap samples were measured and then oven-dried at 50 °C till constant weight to obtain their dry weights (Botwe et al., 2017b). Direct Gamma spectrometric analyses of ^{7}Be (478 keV), ^{234}Th (63.3 keV), ^{210}Pb (^{210}Pb$_{tot}$, 46.5 keV), ^{212}Pb (239 keV), ^{214}Pb (352 keV), ^{214}Bi (609 keV), ^{137}Cs (662 keV) and ^{40}K (1460 keV) were performed at ENEA Marine Environment Research Centre (S. Teresa, Italy). Prior to the Gamma analyses, the sediment core samples were homogenised by grinding and stored air-tight for at least 22 days in plastic vials of standard geometries (5, 10 and 20 g) following Botwe et al. (2017b) to ensure secular equilibrium between the parent nuclides and their short-lived daughter nuclides. The measured activities were decay-corrected to the sediment sampling date.

2.3. Data treatment

Sediment trap-derived settling fluxes (SF, with units of g·cm^{-2}·y^{-1}) were estimated from Eq. (1):

$$SF = \frac{M}{A \times D} \tag{1}$$

where M is the dry accumulated mass of trapped material (g), A is the cross-sectional area of the sediment trap (cm^2) and D is the duration of trap deployment (y).

The water content of the sediment samples was obtained from the difference between the wet and dry weights and expressed as a percentage of the sediment wet weight. The ^{226}Ra activities were indirectly obtained from the average ^{214}Pb and ^{214}Bi activities (Botwe et al., 2017b). For each sediment layer, the ^{210}Pb$_{exc}$ specific activity was obtained by subtracting the ^{226}Ra (supported ^{210}Pb) specific activity from the total ^{210}Pb (^{210}Pb$_{tot}$) specific activity (Corbett et al., 2009). Excess ^{234}Th (^{234}Th$_{exc}$) specific activity was estimated from the total ^{234}Th specific activity by subtracting the background level (the averaged value of concentrations measured downcore, except the topmost layers). Core D required a more complex procedure, since the values measured downcore were not constant. The supported ^{234}Th fraction near the surface was estimated by assuming a constant ^{238}U/^{226}Ra ratio along the

whole core. Bulk densities were evaluated from the determination of the dry weight of the mass contained in a well controlled bulk volume of the sediment, and the mass depths at the centre and at the bottom of each sediment slice determined following Baskaran et al. (2014).

Subsurface sediments may undergo compaction and introduce errors in the determination of sediment depth and age relationships and hence, the estimation of linear sedimentation rates (Abril, 2003; Lu, 2007). Therefore, the activity profiles of ^{7}Be, ^{234}Th$_{exc}$ and ^{210}Pb$_{exc}$ were related to the mass-depth (mass of sediment per unit area, g·cm^{-2}) instead of the linear-depth of the sediment (Erten, 1997; Lu, 2007). Inventories of ^{7}Be were determined for each core by integrating their downcore activities (Giffin and Corbett, 2003; Mullenbach et al., 2004; Palinkas et al., 2005). The simplest SAR modelling approach, defined by the assumptions of constant flux and constant sedimentation rate (CF-CS) without any post-depositional redistribution (Appleby and Oldfield, 1983; Erten, 1997), was applied to the sediment cores to derive very recent (3–8 months) SARs based on the measured ^{7}Be activity profiles.

The TERESA model was applied for the analysis of ^{210}Pb$_{exc}$ versus mass depth profiles. The model fundamentals and its validation against synthetic cores and real data from varved sediments have been described by Abril (2016). In summary, the model stands on the following set of assumptions: (i) ^{210}Pb$_{exc}$ behaves as a particle-associated tracer and new inputs are ideally deposited over the previously existing material; (ii) there is no post-depositional redistribution; (iii) there is continuity of the sequence (i.e., there is not any missing layer by erosion); and (iv) ^{210}Pb$_{exc}$ fluxes are governed by 'horizontal inputs' and thus, there is a statistical correlation between ^{210}Pb$_{exc}$ fluxes and SAR (Abril and Brunskill, 2014). Therefore, for a sediment core which has been sectioned into N slices of mass thickness Δm_i ($i = 1, 2, ... N$), each slice has an associated age interval ΔT_i, a mean SAR value (w_i), and an associated initial specific activity ($A_{0,i}$) corresponding to the activity when that sediment slice was at the sediment-water-interface (SWI).

The TERESA model operates with SAR and initial radionuclide activity distributions, for respectively, w_i and $A_{0,i}$, which closely follow normal distributions around their arithmetic mean values, $\overline{w}$ and $\bar{A}_0$, with standard deviations σ_w and σ_A, respectively. S_w and S_A are, respectively, their normalised values (standard deviation over mean values). Provided a first estimation of $\overline{w}$, $\bar{A}_0$, σ_w and σ_A, the model generates independent random distributions for w_i and $A_{0,i}$; and then an intelligent algorithm solves their best arrangement downcore to fit the experimental ^{210}Pb$_{exc}$ versus the mass depth profile, generating then solutions for the chronological line and for the histories of SAR and sediment fluxes (Abril, 2016). As the result depends on the first estimation of $\overline{w}$, $\bar{A}_0$, σ_w and σ_A, the model applies a mapping technique by iterating the whole process for each parameter varying over a wide range. The error function, Q^2, measures the overall quality of the fit for each individual run of the model (Abril, 2016):

$$Q^2 = \sum_{i=1}^{N} \frac{(A_{th,i} - A_i)^2}{\sigma_i^2}; \chi^2 = Q^2/f \tag{2}$$

where A_i and σ_i are, respectively, the measured value and the analytical error of the radionuclide specific activity at the slice with index i, $A_{th,i}$ being the corresponding value estimated by the model, χ is a measure of the mean distance between the theoretical and experimental profiles in terms of the size of the associated uncertainties, and f is the number of degrees of freedom.

Parametric maps of the χ-function serve to find out the best solution and to support error estimates (Abril, 2016). The typical fundamentals can be applied for error estimates in the four entry parameters (namely $\overline{w}$, σ_w, $\bar{A}_0$, σ_A) through the curvature of the parametric lines in the Q^2 function around the position of the absolute minimum (Bevington and Robinson, 2003). The associated uncertainty in the age at the bottom of each layer, T_j, can then be estimated through the general propagation

law:

$$\sigma^2(T_j) = \left(\frac{\partial T_j}{\partial A_m}\sigma(A_m)\right)^2 + \left(\frac{\partial T_j}{\partial w_m}\sigma(w_m)\right)^2 + \left(\frac{\partial T_j}{\partial \sigma_A}\sigma(\sigma_A)\right)^2 + \left(\frac{\partial T_j}{\partial \sigma_w}\sigma(\sigma_w)\right)^2 \tag{3}$$

Optionally, the model's answers can be better constrained through the use of time markers, when available. As the model-algorithm requires a continuous profile, data from the non-measured sediment slices have been estimated by linear interpolation with ascribed double error-bars to minimise their relative weight in the fit. To avoid the generation of negative values or influencing points when exploring large values of S_w and S_A, lower threshold limits of $0.1\,\bar{A}_0$ and $0.2\,\bar{w}$ have been imposed in all the calculations.

3. Results and discussion

3.1. Estimates of settling fluxes of particulate matter in the Tema Harbour

Table 1 shows the estimated average settling fluxes (SFs) of particulate matter over two sampling depths (top and bottom traps) in the Tema Harbour based on the accumulated dry mass in the sediment traps retrieved every two weeks till the end of the 12-week sampling period. The average SF values over the two sampling depths ranged from 15 (± 3) to 54 (± 18) g·cm^{-2}·y^{-1}, being higher at stations III and IV. About 93% of these SFs (range 84%–96%) correspond to the fraction of particle sizes larger than 63 μm (Table 1). As the typical settling velocities for fine sand and larger particle sizes are over $10\ \mathrm{m\cdot h^{-1}}$ (Eisma, 1993; Ji, 2008), they will be quickly removed from the water column.

From the maximum tidal range of 1.6 m (http://www.tides4fishing.com/af/ghana/tema#_tide_table) and the geometry of the Main Harbour entrance (i.e. 240 m width and 8.5 m mean water depth), it is possible to estimate a maximum cross-sectional averaged water current of about $6\ \mathrm{cm\cdot s^{-1}}$ at the Main Harbour entrance, and a bottom shear stress slightly over 0.07 Pa by applying standard hydrodynamic principles (Periáñez and Abril, 2014; Abril and Periáñez, 2016). This estimated shear stress, which is associated with maximum tidal currents at the Tema Harbour, is over the threshold value (0.06 Pa) for resuspending clays and fine silts (Eisma, 1993; Ji, 2008). But in the inner area of the Main Harbour, the tidal currents are lower and resuspension of sediments is not expected to occur because of the tidal forcing. Nevertheless, ship traffic and particularly the manoeuvres of big cargos and drilling ships can cause remobilisation of large amounts of sediments, as it can be seen from available aerial photographs (e.g. 10/08/2015; Google Earth). Thus, coexistence of sediment deposition and resuspension is expected to occur. Consequently, the obtained SFs may overestimate the SAR values since the material settled within the sediment traps is not allowed to undergo

resuspension, which could occur in real sediments. Thus, the estimated time-averaged SFs from the top and bottom sediment traps at each station represent only a proxy and an upper bound of the expected annually-averaged values at their locations.

Concerning temporal variations, some relative maxima were found at different periods for each station (see Fig. ESM-1, in electronic Supplementary material). The SF values from the top sediment traps were usually comparable or higher than those from the bottom traps, although some exceptions were found at stations I and V. The observed maxima found at different periods for each station did not correspond to a single event of entry of a high mass inflow into the Main Harbour. Moreover, maxima of SFs at the two sampling depths at each sampling station are often registered at different times. This fact points out the importance of local disturbances, which have a highly irregular character both in time and space, and are most likely linked to the manoeuvring of cargo ships. Moreover, from the location of the sampling points, it is expected that station I, at a corner of the Main Harbour, should experience less perturbations and thus capturing lower masses of SF, as indeed found in Table 1. This reveals a complex dynamics of rising clouds of suspended particulate matter (SPM) and settling in the Tema Harbour, interfered by horizontal transport, most likely the one forced by the tidal dynamics.

The mean ($\pm$standard deviation) turbidy values of the surface, mid depth and bottom seawater at the sediment core sampling stations were as follows: core station A = 3.9 (± 0.8) NTU; B = 3 (± 0.6) NTU; C = 3.7 (± 0.7) and D = 4.7 (± 1.1). Although a station-specific ppm (mg·L^{-1}) versus NTU calibration curve was not constructed, from a typical slope of 3.4 ppm/NTU, the turbidity measurements lead to an estimation of the SPM concentration, C, of around 10 ppm. Assuming that this value is representative of the mean environmental conditions at the Tema Harbour and using the SF values in Table 1 (i.e. $SF = v_s C$), the mean values for the settling velocities, v_s, were estimated to be in the range of $(0.5–1.7)10^{-3}\ \mathrm{m\cdot s^{-1}}$, again corresponding to silt and fine sand fractions. These considerations could also provide a gross estimate of the order of magnitude of the expected mean sedimentation rates in the Tema Harbour. From the known tidal range and mean water depth, one could estimate that in each tidal cycle, the Tema Harbour exchanges about 10% of its water volume. If the above SPM concentration of 10 ppm is representative of the marine inflow and the Tema Harbour acts as a huge sediment trap, the expected mean SAR value would be about $6\ \mathrm{g\cdot cm^{-2}\cdot y^{-1}}$. Large local variability is expected around this value due to localised discharge of solids, ship traffic and varying sedimentation yields.

It is worth noting that the SF values from Table 1 captured the prevailing environmental conditions in the SW area of the Tema Harbour during the 12-week deployment period. They represent an upper bound for the sediment mass accumulation rates (SARs) at their respective sampling stations. Rainfall in the sampling area during the sampling period and the preceding month ranged from 0 to 142.3 mm with a mean of 6.1 mm (see Table ESM-1, in electronic Supplementary material). There were no episodic incidents of heavy rainfall, storm runoff or floods during the study period, which could have induced sediment transport into the Tema Harbour and affect the sedimentary regime (Palinkas et al., 2005; Díaz-Asencio et al., 2011).

3.2. Radionuclide and bulk density profiles in sediment cores from Tema Harbour

The mass depth and ^{7}Be, ^{234}Th, ^{210}Pb, ^{226}Ra, ^{212}Pb and ^{137}Cs activity profiles of cores A, B, C and D from the Tema Harbour are shown in Table 2, while Fig. 2 shows the bulk density versus depth profiles for the cores. Table 2 shows that cores A, B and C had similar radionuclide trends, with almost constant downcore ^{210}Pb$_{tot}$ activity (around 200–300 Bq·kg^{-1}), while core D showed large differences in the radionuclide activity profiles with lower activities at intermediate depths (from approximately 15 to 25 cm). For all the cores, the ^{210}Pb$_{exc}$ and ^{137}Cs activity profiles

Table 1

Estimated settling fluxes (SFs) of particulate matter (mean $\pm$ standard error) at five sampling stations in the Tema Harbour (Ghana) based on biweekly accumulated dry mass in sediment traps deployed at two water depths (top and bottom traps) over a period of 12 weeks. The weight fraction (%) of the trapped sediment samples with $\Phi < 63$ μm are also presented. See sampling stations in Fig. 1.

Sampling station	Sediment trap deployment	SF (g·cm^{-2}·y^{-1})	Fraction with $\Phi < 63$ μm (%)
I	Top trap[a]	18 ± 11	8.1
	Bottom trap[b]	21 ± 7	7.6
II	Top trap[b]	25 ± 5	9.4
	Bottom trap[b]	15 ± 3	8.7
III	Top trap[b]	46 ± 16	3.8
	Bottom trap[b]	42 ± 12	3.9
IV	Top trap[b]	54 ± 18	4.5
	Bottom trap[b]	23 ± 8	16.1
V	Top trap[b]	30 ± 13	6.3
	Bottom trap[b]	28 ± 9	5.2

[a] $n = 3$.
[b] $n = 6$.

Table 2
Profiles of mass depth and radioactivity (^{7}Be, ^{234}Th, ^{210}Pb$_{tot}$, ^{226}Ra, ^{212}Pb, ^{40}K and ^{137}Cs) concentrations in sediment cores from Tema Harbour (Ghana). See sampling stations in Fig. 1.

Core ID	Core depth (cm)	[a]Cumulative mass depth (g·cm^2)	Radioactivity concentrations (Bq·kg^{-1})						
			^{7}Be	^{234}Th	^{210}Pb$_{tot}$	^{226}Ra	^{212}Pb	^{40}K	^{137}Cs
A	0–1	0.65	50 ± 9	135 ± 34	296 ± 13	15 ± 2	40 ± 1	317 ± 18	<0.6
	1–2	1.27	29 ± 7	94 ± 32	302 ± 10	12 ± 2	41 ± 1	304 ± 17	<0.6
	2–4	2.39	20 ± 6	28 ± 6	279 ± 10	13 ± 2	36 ± 1	288 ± 15	1.9 ± 0.5
	4–6	4.28	6 ± 3	32 ± 4	319 ± 10	15 ± 1	42 ± 1	313 ± 13	2.1 ± 0.4
	6–8	5.45	5 ± 3	36 ± 4	286 ± 9	14 ± 1	44 ± 1	333 ± 14	1.4 ± 0.4
	8–10	6.62	<6	35 ± 4	251 ± 7	16 ± 1	47 ± 1	336 ± 14	2.0 ± 0.3
	10–12	7.69	<6	31 ± 4	314 ± 9	15 ± 1	28 ± 1	294 ± 11	1.0 ± 0.3
	12–14	9.13	<6	35 ± 3	309 ± 10	15 ± 1	26 ± 1	309 ± 10	1.6 ± 0.3
	16–18	12.67	<6	30 ± 4	300 ± 9	15 ± 1	25 ± 1	271 ± 12	1.7 ± 0.4
	24–26	17.30	<6	39 ± 3	330 ± 9	17 ± 1	25 ± 1	292 ± 10	1.4 ± 0.2
	32–34	22.13	<6	33 ± 3	282 ± 7	15 ± 1	25 ± 1	294 ± 9	1.5 ± 0.3
B	0–1	0.55	61 ± 14	206 ± 30	285 ± 20	11 ± 2	46 ± 3	360 ± 31	<1
	1–2	1.34	17 ± 9	84 ± 46	233 ± 17	13 ± 2	45 ± 2	329 ± 27	2.6 ± 1.0
	2–4	2.71	<9	32 ± 6	245 ± 14	14 ± 1	43 ± 1	323 ± 17	2.1 ± 0.6
	4–6	3.91	<9	43 ± 6	298 ± 15	14 ± 1	29 ± 1	291 ± 15	1.8 ± 0.5
	6–8	5.1	<9	34 ± 9	298 ± 18	16 ± 2	29 ± 1	295 ± 21	1.8 ± 0.7
	8–10	7.3	<9	35 ± 6	284 ± 14	14 ± 1	26 ± 1	285 ± 12	2.0 ± 0.4
	12–14	10.0	<9	40 ± 6	298 ± 15	14 ± 1	27 ± 1	326 ± 15	1.7 ± 0.4
	16–18	12.2	<9	40 ± 6	222 ± 12	13 ± 1	28 ± 1	320 ± 17	0.9 ± 0.4
	22–24	16.6	<9	34 ± 5	175 ± 10	14 ± 1	37 ± 1	324 ± 13	1.8 ± 0.3
	28–30	20.8	<9	29 ± 5	165 ± 10	15 ± 1	37 ± 1	340 ± 14	2.2 ± 0.5
C	0–1	0.26	55 ± 10	196 ± 19	258 ± 17	10 ± 2	48 ± 2	325 ± 28	2.1 ± 0.9
	1–2	0.65	54 ± 12	278 ± 25	276 ± 17	13 ± 2	49 ± 2	375 ± 28	<1
	2–4	2.06	25 ± 5	95 ± 16	242 ± 14	13 ± 1	42 ± 1	314 ± 11	1.2 ± 0.4
	4–6	3.39	<12	36 ± 3	289 ± 16	14 ± 1	43 ± 1	341 ± 11	1.1 ± 0.3
	6–8	4.74	<12	32 ± 4	302 ± 18	14 ± 1	45 ± 1	341 ± 12	1.0 ± 0.4
	8–10	6.31	<12	30 ± 3	182 ± 12	15 ± 1	60 ± 1	396 ± 13	1.3 ± 0.4
	12–14	9.92	<12	34 ± 5	177 ± 13	15 ± 1	59 ± 1	373 ± 15	1.1 ± 0.5
	14–16	11.89	<12	31 ± 5	187 ± 14	15 ± 1	53 ± 1	406 ± 17	1.9 ± 0.5
	16–18	14.14	<12	28 ± 4	155 ± 10	15 ± 1	51 ± 1	453 ± 13	<1
	18–20	16.10	<12	37 ± 4	190 ± 12	17 ± 1	62 ± 1	413 ± 15	1.0 ± 0.3
	32–34	30.95	<12	37 ± 3	203 ± 12	13 ± 1	34 ± 1	404 ± 12	1.3 ± 0.3
	40–42	41.10	<12	37 ± 4	219 ± 13	14 ± 1	35 ± 1	402 ± 12	1.7 ± 0.5
	46–48	48.8	<12	31 ± 5	207 ± 10	16 ± 1	32 ± 1	421 ± 15	1.5 ± 0.3
D	0–1	0.38	126 ± 31	219 ± 37	276 ± 16	17 ± 3	39 ± 1	333 ± 19	2.4 ± 0.8
	1–2	0.94	48 ± 7	276 ± 38	284 ± 13	15 ± 2	40 ± 1	340 ± 19	<1.2
	2–4	2.12	34 ± 9	234 ± 40	269 ± 13	11 ± 2	37 ± 1	321 ± 18	<1.2
	4–6	3.27	19 ± 5	107 ± 15	242 ± 10	12 ± 2	35 ± 1	299 ± 14	<1.2
	6–8	4.82	<6	47 ± 14	217 ± 13	9 ± 2	28 ± 1	302 ± 18	<1.2
	8–10	6.41	<6	25 ± 3	200 ± 8	11 ± 2	25 ± 1	270 ± 13	1.3 ± 0.4
	12–14	10.87	<6	16 ± 3	82 ± 6	7 ± 1	16 ± 0.5	266 ± 11	<0.6
	16–18	17.22	<6	7 ± 2	18 ± 4	5 ± 1	11 ± 0.3	275 ± 9	<0.6
	20–22	24.33	<6	9 ± 3	41 ± 6	4 ± 1	14 ± 0.4	318 ± 13	0.6 ± 0.3
	26–28	33.85	<6	17 ± 2	79 ± 5	9 ± 1	21 ± 0.4	280 ± 10	0.8 ± 0.2
	36–38	48.10	<6	13 ± 2	86 ± 6	7 ± 1	17 ± 0.4	299 ± 11	<0.6
	38–40	49.73	<6	24 ± 4	182 ± 7	12 ± 1	28 ± 0.6	337 ± 12	1.0 ± 0.3

Errors are 1 standard deviation from counting statistics; Minimum Detectable Activity are indicated as <MDA (Bq·kg^{-1}).

[a] At the central point of each sediment slice.

did not reach a zero value in the deeper layers. Moreover, no clearly decreasing ^{210}Pb$_{exc}$ profiles were observed in all four sediment cores.

Fig. 2 shows that bulk density in cores A and B exhibit similar and typical quasi-steady compaction profiles broken by some intermediate relative peaks. Core C showed a trend of increasing bulk density downcore with anomalous low values at the top 0–2 cm layer. Core D showed a distinct structure, with higher values of bulk density below the 15 cm depth. Thus, the data on bulk density suggest highly dynamic and non-steady sedimentary conditions at the study site (Abril, 2003). It is worth noting that high values of bulk density are typically associated with the presence of coarser grain-sizes, which have lower specific activities of surface-bound radionuclides.

3.3. Inventories and fluxes of ^{7}Be and ^{7}Be-derived sediment accumulation rates

The measurement of ^{7}Be specific activities in the top layer of a sediment core is usually considered as a quality test for the complete surface recovery of the core, which is necessary for dating (Erten et al., 1985; Erten, 1997). In the Tema Harbour, it was possible to measure ^{7}Be in several sediment slices downcore (Table 2). This provided an opportunity to determine the very recent SAR values over the past 6–8 months under some simplifying assumptions. The ^{7}Be inventories (see Table 3) ranged from 470 (±110) to 1360 (±170) Bq·m^{-2}, core D being richer in ^{7}Be than the other cores. The ^{7}Be inventories in the Tema Harbour sediments were higher, but comparable to the values reported by Olsen et al. (1985) for coastal sediments from Virginia and Tennessee (370–740 Bq·m^{-2}). The ^{7}Be inventories in the Tema Harbour sediments were also comparable to, but lower than the values reported for (1) sediments of the Neuse and Pamlico River Estuaries (33–97 Bq·m^{-2}) by Giffin and Corbett (2003), (2) sediments of the Eel Canyon, northern California (5780–12,000 Bq·m^{-2}) by Mullenbach et al. (2004), and (3) sediments from Po River delta, Adriatic Sea (190–5420 Bq·m^{-2}) by Palinkas et al. (2005). The fluxes of ^{7}Be onto the SWI, assumed to be constant, were estimated from the product of the ^{7}Be inventories and the radioactive decay constant. They varied from 2200 (±500) to 6500 (±800) Bq·m^{-2}·y^{-1} (Table 3). The spatial variability in ^{7}Be values in the Tema Harbour may be due to the fact that uptake of atmospheric ^{7}Be by SPM mediates its fluxes onto the SWI. A large spatial variability in ^{7}Be inventories is a common feature of coastal sediments, which has been
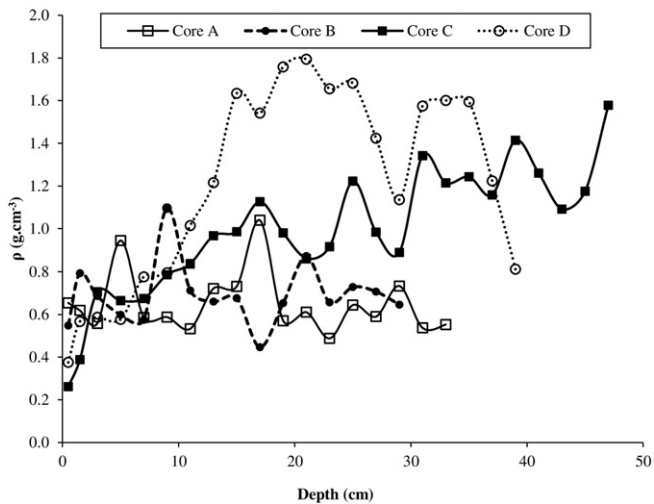
Fig. 2. Bulk density (ρ) versus depth profiles for sediment cores A, B, C and D sampled from Tema Harbour (Ghana).

Fig. 3. ^{7}Be versus mass depth profiles of sediment cores A, B, C and D sampled from Tema Harbour (Ghana). Error bars represent 1-σ counting uncertainties.

previously reported in the scientific literature (Rose and Kuehl, 2010; Kolker et al., 2012).

Fig. 3 shows that ^{7}Be versus mass depth profiles in sediment cores A and D followed an exponential decay at a confidence level of over 90%, while for cores B and C the number of data points is not statistically significant. Table 3 reports the ^{7}Be-derived SAR values, assuming the applicability of the CF-CS model. The SAR values were in the range of 2.5–9.0 g·cm^{-2}·y^{-1}, and were much lower than the sediment trap-derived SFs (Table 1). This observation points out the important role of sediment resuspension in the sedimentation process at the Tema Harbour, as expected from the aerial photographs (see Section 3.1). Nevertheless, these values have to be taken as a first estimate of the order of magnitude of SARs in Tema Harbour. The reported uncertainties in Table 3 come from a numerical fitting which does not account for the uncertainties in the radionuclide specific activities. But "the model errors" arising from a partial accomplishment of the involved assumptions may be more relevant. Thus, the ^{7}Be versus mass-depth profiles could be mediated by mixing, diffusion or non-ideal depth deposition of fluxes, which would result in somewhat lower SAR values than the above estimates. Particularly, the assumption of a constant flux is problematic for ^{7}Be due to its short half-life (Taylor et al., 2013).

It has been shown for different geographical latitudes that the atmospheric deposition of ^{7}Be is well correlated with rainfall (Pham et al., 2013). Rainfall in southern Ghana is higher during the rainy season (April–June and September–October) and minimum during the dry season (November–March and July–August). Unusually high rainfall values of about 100 mm were recorded for both February and March 2015, while only 30–40 mm was recorded in January 2015 (https://jbaidoowilliams.com/2015/10/20/el-nino-2015-rainfall-fears/). Although a system time-averaged integration of fluxes has been described (Robbins et al., 2000), the assumption of constant fluxes of ^{7}Be may be an oversimplification. On the other hand, the short penetration depth of ^{7}Be
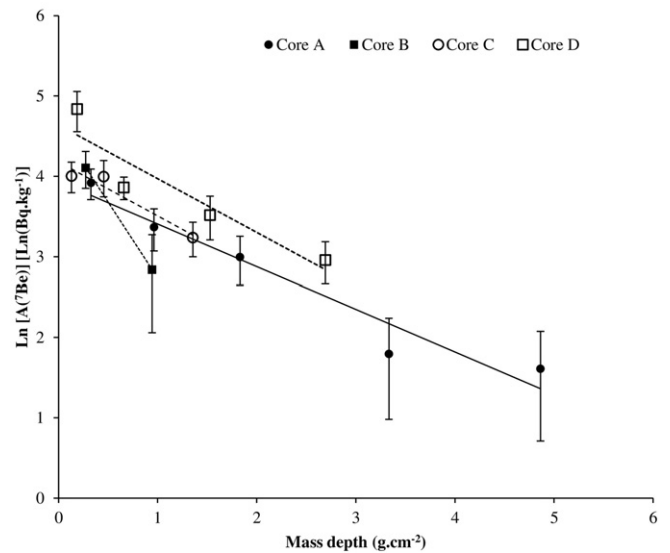
Table 3
^{7}Be inventories and fluxes onto the sediment-water interface (SWI) and ^{7}Be-derived sediment accumulation rate (SAR) values in sediment cores from Tema Harbour (Ghana).

Core	^{7}Be inventory (Bq·m^{-2})	^{7}Be flux onto SWI (Bq·m^{-2}·y^{-1})	^{7}Be-derived SAR[a] (g·cm^{-2}·y^{-1})
A	900 ± 120	4300 ± 600	9.0 ± 1.3
B	470 ± 110	2200 ± 500	2.5 ± nd
C	710 ± 90	3400 ± 400	7.1 ± 1.8
D	1360 ± 170	6500 ± 800	7.1 ± 2.0

nd: not determined.
[a] From a CF-CS model.

in the core makes its profile more sensitive to surficial processes such as the non-ideal deposition described by Abril and Gharbi (2012).

The ^{234}Th activity versus mass depth profiles (Table 2) showed a near-constant background level along the cores at the 2–3 cm upper sediment slices. This is consistent with the high SAR values estimated from the ^{7}Be data.

3.4. Analysis of $^{210}Pb_{exc}$ fluxes onto the SWI and mixing

From Table 2, the surficial specific activities of ^{210}Pb$_{exc}$ (~300 Bq·kg^{-1}) were over one order of magnitude higher than those reported by Nyarko et al. (2016) for sediment cores from the Pra and Volta estuaries in Ghana. The difference can be explained in terms of the granulometry of the sediments, with a large component of the inputs linked to the small grain-size SPM supplied by the tidal inflow. For the theoretical basis of the relationship among radionuclide specific activities and particle size, see Abril and Fraga (1996) and Abril (1998). The analysed cores were too short to allow any reliable estimation of the total ^{210}Pb$_{exc}$ inventories required for the application of the constant rate of supply (CRS) model. The low values and large uncertainties in the ^{137}Cs data did not allow any proper identification of chrono-stratigraphic horizons. Moreover, cores A, C and D did not follow any clear monotonic exponential trend of decrease (Fig. 4) and thus, the application of the CF-CS model for deriving SAR values was not reliable.

The SAR values derived from ^{7}Be data, along with the ^{210}Pb$_{exc}$ specific activities in the upper sediment layers can be used to obtain a first estimate of the ^{210}Pb$_{exc}$ fluxes onto the SWI if any post-depositional remobilization is discarded. Thus, for core A, this resulted in a flux onto the SWI of 25.6 kBq·m^{-2}·y^{-1}, being two orders of magnitude higher than the expected atmospheric deposition of ^{210}Pb$_{exc}$ in the Tema Harbour area (typically in the range of 100–200 Bq·m^{-2}·y^{-1}). This means that fluxes of ^{210}Pb$_{exc}$ onto the SWI must be governed by fluxes of matter (Abril and Brunskill, 2014). Furthermore, the models handling high diffusion coefficients and null or low SAR values under steady-state conditions could roughly fit the profiles from cores A, B and C (not shown). However, these models require fluxes of up to 100 kBq·m^{-2}·y^{-1} to enter into the SWI (mostly in the dissolved form), which cannot be supplied by atmospheric deposition.

About mixing, on the other hand, no observational evidence of bioturbation was available that would induce sediment mixing over large mass depths. Some degree of horizontal and vertical mixing may, nevertheless, exist due to the remobilization forced by ship displacements. But

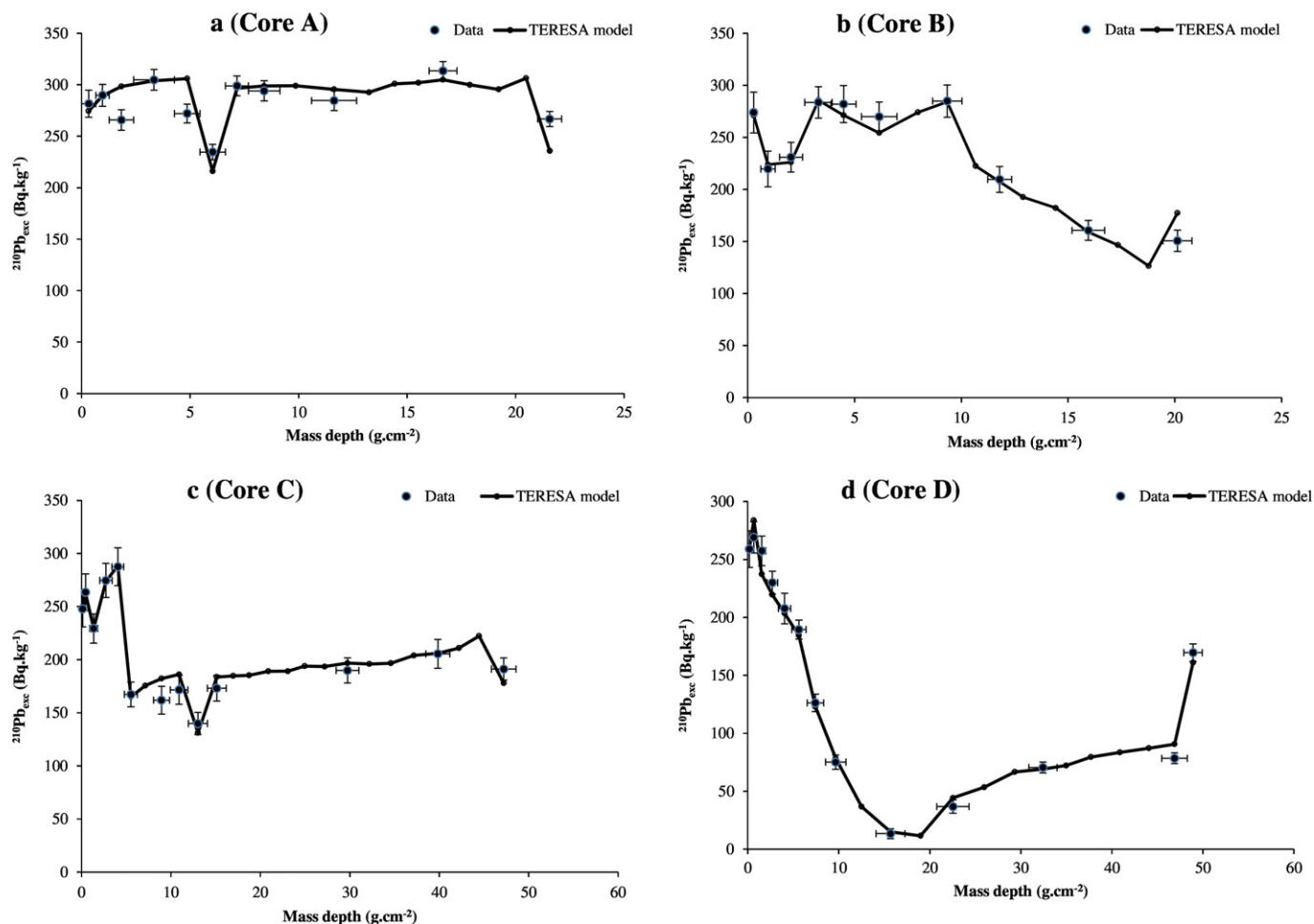**Fig. 4.** $^{210}Pb_{exc}$ versus mass depth profile for (a) core A, (b) core B, (c) core C and (d) core D in the Tema Harbour (Ghana). Vertical bars correspond to the associated uncertainties (1-σ), while the horizontal ones define the mass depth interval of each sediment slice. The numerical solution generated by the TERESA model is plotted as points at the centre of each slice interval (continuous line is only for guiding-eyes).

as data from sediment traps integrate a large number of such events, mixing in the sediments is not expected to exceed the 1–2 cm surface layer. About 70 vessels enter and leave the Tema Harbour weekly, most of them being cargo, tug and tanker vessels; and they follow well-defined tracks within the harbour (http://www.marinetraffic.com/en/ais/details/ports/86/Ghana_port:TEMA). In contrast, the depth profiles of ^7Be and ^{234}Th in the sampling sites showed sharp gradients in the 0–2 cm layers, which are not compatible with a well-mixed layer. The hypothesis of mixing can thus be discarded as a main governing factor to explain the observed profiles. As the cores were sampled out of the dredged area (Fig. 1), they must have preserved a sequence of continuous sediment deposition.

3.5. Analyses of ^{210}Pb profiles and estimation of SARs using the TERESA model

The hypothesis of varying, but statistically correlated, fluxes of matter and $^{210}Pb_{exc}$ onto the SWI seems reasonable for the Tema Harbour and thus, the conditions for applying the TERESA model can be met. Fig. ESM-2 (in electronic Supplementary material) shows the computed maps for the χ function (see Section 2.3) in the ($\overline{A}_0$, $\overline{w}$) and (S_A - S_W) spaces for the four studied cores with the TERESA model. They have been computed with the stand-alone version of the model and with the basic method-A (Abril, 2016), and they show relatively well defined valleys which determine the parameter values along with their associated fitting uncertainties, reported in Table 4. The computed $^{210}Pb_{exc}$ vs.

mass depth profiles are shown in Fig. 4(a–d), and they match the experimental data with the χ values reported in Table 4. Finally, the resulting chronologies for the four cores are shown in Fig. 5.

3.6. Analyses of sediment cores A, B and C

Data from sediment core A showed the highest values of $^{210}Pb_{exc}$ specific activities and they remained almost constant downcore. The TERESA model produced a reasonable fit to the data with arithmetic means of 364 Bq·kg^{-1} and 1.62 g·cm^{-2}·y^{-1} and normalised standard deviations of 0.175 and 0.384 for the initial specific activity and SAR, respectively. It is worth noting that there were no alternative valley regions in the χ surface, and the fit, although not especially good, was well constrained, as inferred from the low fitting uncertainties (which are related to the curvature of the χ-surface along the parametric lines). There was a trend of

Table 4
Entry parameters of the TERESA model and fitting-error estimates[a] for the investigated cores from the Tema Harbour, where $\overline{A}_0$ (Bq·kg^{-1}) is the mean initial concentration, $\overline{w}$ is the mean SAR value (g·cm^{-2}·y^{-1}) and S_A, S_w are the corresponding relative standard deviations.

Core	$\overline{A}_0$	$\overline{w}$	S_A	S_w	χ
A	364.0 ± 0.2	1.620 ± 0.008	0.175 ± 0.003	0.384 ± 0.006	1.90
B	262.0 ± 1.0	1.87 ± 0.07	0.169 ± 0.009	0.322 ± 0.024	0.96
C	253.0 ± 1.2	3.27 ± 0.21	0.200 ± 0.010	0.27 ± 0.08	0.61
D	152.5 ± 0.1	4.080 ± 0.004	0.600 ± 0.001	0.990 ± 0.003	1.09

[a] Through the second derivative of the Q^2 function (Bevington and Robinson, 2003).
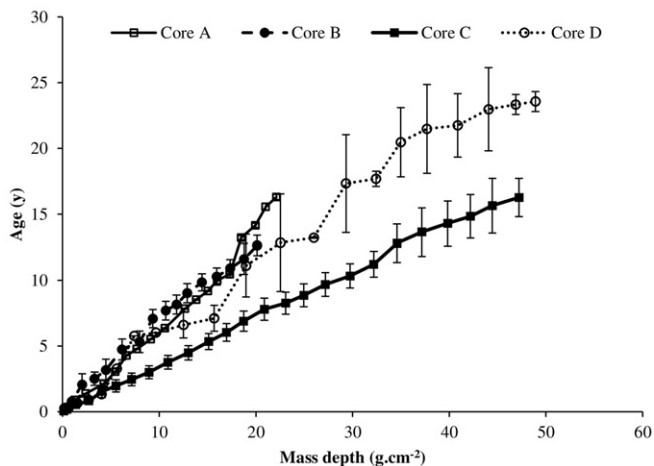
Fig. 5. Chronologies estimated by the TERESA model for the investigated sediment cores from the Tema Harbour (Ghana) along with their corresponding uncertainty intervals (from the propagation of error associated to the fitting parameters of Table 4).

decreasing radionuclide specific activities in recent dates, which compensates for the radioactive decay in the deeper layers and explains the observed profile. The age of the deepest measured sediment slice (32–34 cm) was estimated at 16 y, which implies a time-averaged SAR of 1.4 $g \cdot cm^{-2} \cdot y^{-1}$ (or 2.1 $cm \cdot y^{-1}$). The time-averaged SAR is used likewise the CRS dating model in order to make these values comparable with literature data.

The chronological line generated by the TERESA model for sediment core B ran close to the one from core A (Fig. 5), with a slightly higher value of SAR and lower initial radionuclide specific activity (arithmetic means of 1.87 $g \cdot cm^{-2} \cdot y^{-1}$ and 262 $Bq \cdot kg^{-1}$, respectively). The age of the deepest measured sediment slice (28–30 cm) was estimated at 13 y, which implies a time-averaged SAR of 1.6 $g \cdot cm^{-2} \cdot y^{-1}$ (or 2.4 $cm \cdot y^{-1}$).

Sediment core C showed a $^{210}Pb_{exc}$ profile with a distinct sub-surface peak followed by a plateau area, and it was well reproduced by the TERESA model (Fig. 4c). The arithmetic mean value for the initial specific activity was close to the one for sediment core B, but the SAR value was noticeably higher. The age of the deepest measured sediment slice (46–48 cm) was estimated at 16 y (with a time-averaged SAR of 2.9 $g \cdot cm^{-2} \cdot y^{-1}$ or 3.0 $cm \cdot y^{-1}$). The distinct peak extended up to a mass-depth of 4.06 $g \cdot cm^{-2}$, for which the TERESA-derived age was 1.5 (± 0.5) y (Fig. 5). The building of the wharf structure between 2013 and 2014 might have changed the local sedimentological conditions. Under the new conditions, the radionuclides content in sediment core C tends to the values found in sediment core A (see Table 2). This implies that before the deployment of the pillars, the fluxes of matter on the site of sediment core C were contributed by both marine inflow and some local sources, which resulted in higher bulk densities (Fig. 2), higher SAR (Table 4), lower $^{210}Pb_{exc}$ activity content and some higher ^{40}K specific activities (see Table 2). The sharp discontinuity in radionuclides profiles at the mass-depth of 4.06 $g \cdot cm^{-2}$ confirms the hypothesis of negligible post depositional processes.

3.7. Analysis of sediment core D

Sediment core D showed a complex $^{210}Pb_{exc}$ profile with high specific activities around 270 $Bq \cdot kg^{-1}$ at the top layers, which decline till 13 $Bq \cdot kg^{-1}$ at a mass depth of 17 $g \cdot cm^{-2}$ and then increase downcore till 170 $Bq \cdot kg^{-1}$ (Fig. 4d). The area with low $^{210}Pb_{exc}$ specific activities was associated with high values of bulk density (Fig. 2). The TERESA model was able to reasonably reproduce the complex $^{210}Pb_{exc}$ profile of sediment core D ($\chi = 1.09$, see Fig. 4d) with arithmetic means of initial activities and SAR which are roughly 2/5 and 5/2 of the ones found for sediment core A (Table 4). A large variability was ascribed to both

values with reference normalised standard deviations of 0.60 and 0.99, respectively. The computed initial specific activities was plotted versus mass depths to display a U-shape with a minimum mass depth around 17–21 $g \cdot cm^{-2}$ (age 11–13 y). This induced a huge dilution effect, most likely attributable to local sources of matter with negligible $^{210}Pb_{exc}$ content, so the mean value of the flux onto the SWI was 6.2 $kBq \cdot m^{-2} \cdot y^{-1}$, as in sediment core A. As in the case of sediment core C, these local sources also resulted in higher bulk densities (Fig. 2) and the overall higher SAR (Table 4). The variability in SAR was very high, but randomly distributed, which resulted in a relatively uniform chronological line (Fig. 5). The age of the deepest measured sediment slice (38–40 cm) was estimated at 24 y, which implies a time-averaged SAR of 2.1 $g \cdot cm^{-2} \cdot y^{-1}$ (or 1.7 $cm \cdot y^{-1}$).

The above interpretation can be further supported by the analysis of the $^{234}Th_{exc}$ profile in sediment core D. When excluding the topmost layers, the ^{234}Th concentrations were almost constant downcore with almost uniform $^{234}Th/^{226}Ra$ isotopic ratios, having mean ($\pm$ standard deviation) values of 2.24 (± 0.17), 2.57 (± 0.45), 2.28 (± 0.33) and 1.72 (± 0.15) for sediment cores A, B, C and D, respectively. When comparing the concentrations of ^{234}Th and ^{226}Ra along the four sediment cores, it is striking to note that in core D, their values were about a factor of 2 lower in the central layers associated with low values of $^{210}Pb_{exc}$ and high bulk density values. The low radionuclide specific activities, while keeping the isotopic ratios, can only be explained by the dilution of naturally settling material with other sources of matter. A similar effect of dilution is observed for ^{226}Ra and ^{212}Pb isotopes, which show an increasing trend in the top sediment layers (Fig. 6). This means that the dilution effect progressively vanished during the last six years, according to the chronology reported in Fig. 5. Their concentrations at the recent SWI converge to the ones found for sediment core A (see Table 2). The dilution was not so apparent for ^{40}K (Fig. 6) and thus this radionuclide should be present in the local source of matter at concentrations somewhat lower than those found in sediment core A.

The reported uncertainties in the entry parameters of the TERESA model (Table 4) came from the fitting procedure, while the ones reported with the chronologies (Fig. 5) came from their propagation. As with all the models, there are other sources of uncertainty associated with the partial accomplishment of the model assumptions. In the TERESA model, the reference normal distributions for initial activities and SAR (truncated with the minimum threshold values) are only a proxy to the real ones occurring in nature. The incomplete sequence of measurements make interpolations necessary, and the absence of independent and well distributed chronostratigraphic marks did not allow the use of the complete model capabilities (Abril, 2016).
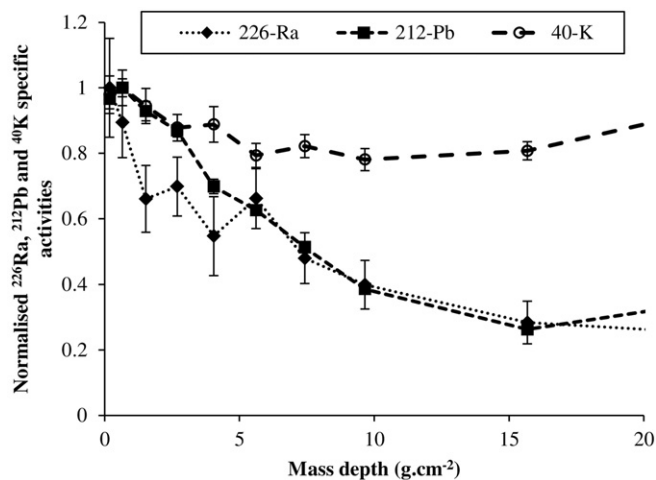

Fig. 6. Normalised (to their maximum value) ^{226}Ra, ^{212}Pb and ^{40}K specific activities versus mass depth for sediment core D sampled from the Tema Harbour (Ghana).

3.8. Comparison of SAR values among sediment cores A, B, C and D

Despite the above limitations, the TERESA model was able to depict a good scenario for the sedimentation in the Tema Harbour, with overall SAR values with time-averages in the range of 1.4–3.0 $g \cdot cm^{-2} \cdot y^{-1}$. The analysed sediment core lengths were too short and only captured the last 13–24 years of sedimentation (extreme values for sediment cores B and D, respectively). Sediment cores A and B seemed to capture the less perturbed conditions, and they were governed by the marine inflow of SPM with higher $^{210}Pb_{exc}$ specific activities and most likely linked to a finer granulometry. The TERESA model captured a change in the sedimentary conditions for sediment core C, whose age is in reasonable agreement with the time of deployment of the concrete pillars of the new wharf structure. According to the model results, the previous sedimentary environment around sediment core C also received matter with lower radionuclide activity content from local sources, leading to high SAR and high bulk densities. A more extreme change in sedimentary conditions was observed for the sediment core D site, which is located in the harbour area transited by cargo ships. Here, the TERESA model reproduced a noticeable dilution effect also attributable to the mixing of the marine inflow of SPM with local sources of matter that had low specific activities of $^{210}Pb_{exc}$, ^{226}Ra, ^{234}Th and ^{212}Pb.

3.9. Comparison of the TERESA- and ^7Be-derived SARs

The SAR values derived from the TERESA model were of the same order, but noticeably lower than those estimated from the ^7Be data. As discussed above, the assumption of a constant flux may be an oversimplification for ^7Be and so the SAR was not constant. The overestimation of SAR calculated by ^7Be is most likely the major effect of a mass-depth penetration of a fraction of the ^7Be fluxes (non-ideal deposition as described by Abril and Gharbi, 2012). A fraction of the radiotracer flux crossing the SWI exists in dissolved form or attached to small grain-size fractions. This fraction can penetrate through the connected water pores and be distributed at depth instead of being deposited over the previously existing material. This effect has been widely observed for ^7Be in soils (Taylor et al., 2013), riverine floodplain sediments (Sommerfield et al., 1999), and in marine environments (Rose and Kuehl, 2010). Thus, as a demonstration of the concept, Fig. 7 plots the results from a numerical simulation for the ^7Be distribution in core A using the SAR value from the TERESA model, and a non-ideal deposition
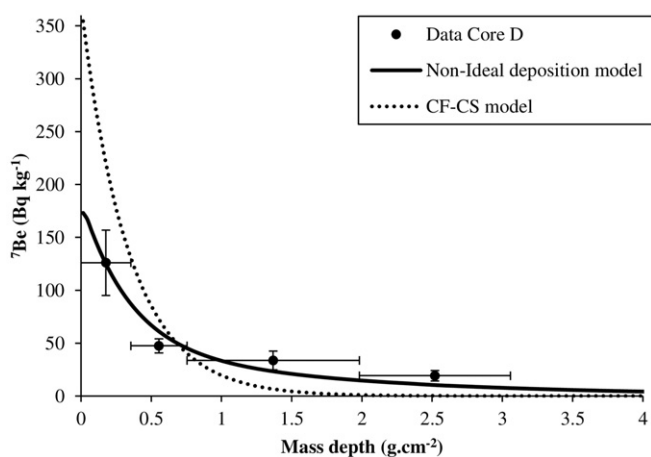
described by factors g = 0.5 and α = 0.6 $g^{-1} \cdot cm^2$ (see Abril and Gharbi, 2012). The plot was compared against the corresponding exponential decline from a CF-CS model with ideal deposition under the same sedimentological conditions. Fig. 7 confirms non-ideal deposition may seriously limit the applicability of short-lived radionuclides to radiometric dating of recent sediments, while its effects less affected $^{210}Pb_{exc}$: it produced slight distortions in the upper layers, where subsurface maxima are often found (Abril and Gharbi, 2012). The TERESA model compensates for these effects on the $^{210}Pb_{exc}$ profile through an equivalent variability in initial radionuclide activities and/or SAR, as shown in Abril (2016) with the TERESA chronology for a varved sediment core from the Santa Barbara Basin (California, USA) for which non-ideal sediment deposition has been described by Abril and Gharbi (2012).

The time-averaged SAR values found in the tropical coastal Tema Harbour by the TERESA model (1.4–3.0 $g \cdot cm^{-2} \cdot y^{-1}$) were very high when compared with most of the literature data for lacustrine and coastal environments from other climatic regions. Accounting for the high bulk density of the sediments in the Tema Harbour, the accretion rates were in the range of 1.7–3 $cm \cdot y^{-1}$. Also, these accretion rates were higher than values reported in the scientific literature for harbour areas, e.g. 0.57 $cm \cdot y^{-1}$ in the Tanjung Pelepas Harbour, Malaysia (Yusoff et al., 2015); 1.2 $cm \cdot y^{-1}$ in the Victoria Harbour, Hong Kong (Tang et al., 2008); 0.2–2 $cm \cdot y^{-1}$ for Sydney Harbour, Nova Scotia, Canada (Smith et al., 2009). This implies that typical coring devices, allowing for core lengths below 1 m may be too short for recovering the whole $^{210}Pb_{exc}$ inventory. This, along with irregular non-monotonic profiles, seriously limited the application of most of the conventional ^{210}Pb-based dating models in the studied Tema Harbour cores. The accretion rates in the Tema Harbour are, nevertheless, only of moderate concern for the harbour sustainability, i.e. filling up the harbour basin and imposing a need for dredging. If these conditions had prevailed since its construction in 1962, the net accretion around the studied sites would have been in the range of 0.9–1.6 m, which is in agreement with the partial dredging conducted in 2014.

4. Conclusions

Settling fluxes and sedimentation rates in coastal Tema Harbour (Ghana) have been investigated based on accumulated dry mass in sediment traps and radionuclide (^7Be, ^{234}Th, ^{210}Pb, ^{226}Ra, ^{40}K, ^{212}Pb and ^{137}Cs) profiles in four sediment cores. The average settling fluxes ranged from 15 ($\pm$3) to 54 ($\pm$18) $g \cdot cm^{-2} \cdot y^{-1}$, showing spatial and temporal variations from which a complex dynamics of suspended particulate matter in the Tema Harbour is inferred. The analysed sediment cores were too short to allow any reliable estimation of SARs in the Tema Harbour based on the $^{210}Pb_{exc}$ inventories and traditional dating models (CF-CS and CRS). The ^{210}Pb-based TERESA model was successfully applied to depict a good scenario for sedimentation rates in the Tema Harbour over the past 13–24 y, with overall time-averaged SAR values in the range of 1.4–3.0 $g \cdot cm^{-2} \cdot y^{-1}$. These SAR values imply sediment accretion rates of 1.7–3 $cm \cdot y^{-1}$ in the Tema Harbour, which poses a moderate problem of sustainability for its management.

Fig. 7. Numerical simulation for the ^7Be distribution in sediment core D using the SAR value from the TERESA model, and a non-ideal deposition described by factors g = 0.5, α = 0.6 $g^{-1} \cdot cm^2$ (see Abril and Gharbi, 2012), and the simplifying assumption of constant flux. The plot is compared against the corresponding exponential decline from a CF-CS with ideal deposition under the same sedimentological conditions. Horizontal bars correspond to the depth intervals.

References

Abril, J.M., 1998. Basic microscopic theory of the distribution, transfer and uptake kinetics
of dissolved radionuclides by suspended particulate matter - part I: theory develop-ment. J. Environ. Radioact. 41 (3), 307–324.

Abril, J.M., 2003. A new theoretical treatment of compaction and the advective-diffusive
processes in sediments: a reviewed basis for radiometric dating models. J. Paleolimnol. 30 (4), 363–370.

Abril, J.M., 2004. Constraints on the use of ^{137}Cs as a time-marker to support CRS and SIT chronologies. Environ. Pollut. 129 (1), 31–37.

Abril, J.M., 2016. A ^{210}Pb-based chronological model for recent sediments with random entries of mass and activities: model development. J. Environ. Radioact. 151, 64–74.

Abril, J.M., Brunskill, G.J., 2014. Evidence that excess ^{210}Pb flux varies with sediment accumulation rate and implications for dating recent sediments. J. Paleolimnol. 52 (3), 121–137.

Abril, J.M., Fraga, E., 1996. Some physical and chemical features of the variability of K_d distribution coefficients for radionuclides. J. Environ. Radioact. 30 (3), 253–270.

Abril, J.M., Gharbi, F., 2012. Radiometric dating of recent sediments: beyond the boundary conditions. J. Paleolimnol. 48 (2), 449–460.

Abril, J.M., Periáñez, R., 2016. Revisiting the time scale and size of the Zanclean flood of the Mediterranean (5.33 Ma) from CFD simulations. Mar. Geol. 382, 242–256.

Akrasi, S., 2011. Sediment discharges from Ghanaian rivers into the sea. West Afr J. App. Ecol. 18 (1), 1–13.

Alonso-Hernandez, C., Diaz-Asencio, M., Muñoz-Caravaca, A., Delfanti, R., Papucci, C., Ferretti, O., Crovato, C., 2006. Recent changes in sedimentation regime in Cienfuegos Bay, Cuba, as inferred from ^{210}Pb and ^{137}Cs vertical profiles. Cont. Shelf Res. 26 (2), 153–167.

Appleby, P.G., Oldfield, F., 1978. The calculation of lead-210 dates assuming a constant rate of supply of unsupported ^{210}Pb to the sediment. Catena 5, 1–8.

Appleby, P.G., Oldfield, F., 1983. The assessment of ^{210}Pb data from sites with varying sediment accumulation rates. Hydrobiologia 103 (1), 29–35.

Barneveld, H., Hugtenburg, J., 2008. Feasibility study for implementation of sedimentation reduction measures in river harbours. RCEM, pp. 1187–1192.

Baskaran, M., Nix, J., Kuyper, C., Karunakara, N., 2014. Problems with the dating of sediment core using excess ^{210}Pb in a freshwater system impacted by large scale watershed changes. J. Environ. Radioact. 138, 355–363.

Bellucci, L.G., Giuliani, S., Romano, S., Albertazzi, S., Mugnai, C., Frignani, M., 2012. An integrated approach to the assessment of pollutant delivery chronologies to impacted areas: Hg in the Augusta Bay (Italy). Environ. Sci. Technol. 46 (4), 2040–2046.

Bevington, P.A., Robinson, D.K., 2003. Data Reduction and Error Analysis for the Physical Sciences. 3rd Edition. McGraw-Hill, New York.

Bloesch, J., Burns, N., 1980. A critical review of sedimentation trap technique. Schweiz. Z. Hydrol. 42 (1), 15–55.

Botwe, B.O., De Schamphelaere, K., Schipper, C.A., Teuchies, J., Blust, R., Nyarko, E., Lens, P.N.L., 2017a. Integrated hazard, risk and impact assessment of tropical marine sediments from Tema Harbour (Ghana). Chemosphere 177, 24–34.

Botwe, B.O., Kelderman, P., Nyarko, E., Lens, P.N.L., 2017b. Assessment of DDT, HCH and PAH contamination and associated ecotoxicological risks in surface sediments of coastal Tema Harbour (Ghana). Mar. Pollut. Bull. 115 (1–2), 480–488.

Botwe, B.O., Schirone, A., Delbono, I., Barsanti, M., Delfanti, R., Kelderman, P., Nyarko, E., Lens, P.N.L., 2017c. Radioactivity concentrations and their radiological significance in sediments of the Tema Harbour (Greater Accra, Ghana). J. Radiat. Res. Appl. Sci. 10 (1), 63–71.

Brisson, L.N., Wolfe, D.A., Staley, M., 2014. Interferometric swath bathymetry for large scale shallow water hydrographic surveys. Canadian Hydrographic Conference, pp. 1–18.

Brucker, S., Clarke, J.H., Beaudoin, J., Lessels, C., Czotte, K., Loschiavo, R., Iwanowska, K., Hill, P., 2007. Monitoring flood-related change in bathymetry and sediment distribution over the Squamish Delta, Howe Sound, British Columbia. U.S. Hydrographic Conference, pp. 1–16.

Buesseler, K.O., Antia, A.N., Chen, M., Fowler, S.W., Gardner, W.D., Gustafsson, O., Harada, K., Michaels, A.F., van der Loeff M, Rutgers, Sarin, M., 2007. An assessment of the use of sediment traps for estimating upper ocean particle fluxes. J. Mar. Res. 65 (3), 345–416.

Caroll, J., Lerche, I., 2003. Sedimentary Processes: Quantification Using Radionuclides. Elsevier.

Corbett, D.R., Walsh, J.P., Marciniak, K., 2009. Temporal and spatial variability of trace metals in sediments of two adjacent tributaries of the Neuse River Estuary, North Carolina, USA. Mar. Pollut. Bull. 58 (11), 1739–1747.

Díaz-Asencio, M., Alvarado, J.C., Alonso-Hernández, C., Quejido-Cabezas, A., Ruiz-Fernández, A., Sanchez-Sanchez, M., Hernández-Albernas, J.I., Eriksson, M., Sanchez-Cabeza, J., 2011. Reconstruction of metal pollution and recent sedimentation processes in Havana Bay (Cuba): a tool for coastal ecosystem management. J. Hazard. Mater. 196, 402–411.

Eisma, D., 1993. Suspended Matter in the Aquatic Environment. Springer-Verlag.

Erten, H., 1997. Radiochronology of lake sediments. Pure Appl. Chem. 69 (1), 71–76.

Erten, H., Von Gunten, H., Rössler, E., Sturm, M., 1985. Dating of sediments from Lake Zurich (Switzerland) with 210 Pb and 137 Cs. Swiss J. Hydrol. 47 (1), 5–11.

Fuller, C., van Geen, A., Baskaran, M., Anima, R., 1999. Sediment chronology in San Francisco Bay, California, defined by ^{210}Pb, ^{234}Th, ^{137}Cs, and ^{239,240}Pu. Mar. Chem. 64 (1), 7–27.

Giffin, D., Corbett, D.R., 2003. Evaluation of sediment dynamics in coastal systems via short-lived radioisotopes. J. Mar. Syst. 42 (3), 83–96.

Green, M.O., Coco, G., 2014. Review of wave-driven sediment resuspension and transport in estuaries. Rev. Geophys. 52 (1), 77–117.

IAEA, 2004. Sediment distribution coefficients and concentration factors for biota in the marine environment. Technical Reports Series No. 422. International Atomic Energy Agency.

Ji, Z.G., 2008. Hydrodynamics and Water Quality: Modelling Rivers, Lakes and Estuaries. Wiley.

Kelderman, P., 2012. Sediment pollution, transport, and abatement measures in the city canals of delft, The Netherlands. Water Air Soil Pollut. 223 (7), 4627–4645.

Kelderman, P., Ang'weya, R., De Rozari, P., Vijverberg, T., 2012. Sediment characteristics and wind-induced sediment dynamics in shallow Lake Markermeer, the Netherlands. Aquat. Sci. 74 (2), 301–313.

Khaba, L., Griffiths, J.A., 2017. Calculation of reservoir capacity loss due to sediment deposition in the Muela reservoir, Northern Lesotho. Int. Soil Water Conserv. Res. 5, 130–140.

Kolker, A.S., Miner, M.D., Weathers, H.D., 2012. Depositional dynamics in a river diversion receiving basin: the case of the West Bay Mississippi River Diversion. Estuar. Coast. Shelf Sci. 106, 1–12.

Lepland, A., Andersen, T.J., Lepland, A., Arp, H.P.H., Alve, E., Breedveld, G.D., Rindby, A., 2010. Sedimentation and chronology of heavy metal pollution in Oslo Harbour, Norway. Mar. Pollut. Bull. 60 (9), 1512–1522.

Leys, V., Mulligan, R.P., 2011. Modelling coastal sediment transport for harbour planning: selected case studies. INTECH.

Lu, X., 2007. A note on removal of the compaction effect for the ^{210}Pb method. Appl. Radiat. Isot. 65 (1), 142–146.

Mullenbach, B., Nittrouer, C., Puig, P., Orange, D., 2004. Sediment deposition in a modern submarine canyon: Eel Canyon, northern California. Mar. Geol. 211 (1), 101–119.

Nyarko, E., Klubi, E., Laissaoui, A., Benmansour, M., 2016. Estimating recent sedimentation rates using lead-210 in tropical estuarine systems: case study of Volta and Pra estuaries in Ghana, West Africa. J. Oceanogr. Mar. Res. 4 (1), 141–145.

Olsen, C.R., Larsen, I.L., Lowry, P.D., Cutshall, N.H., Todd, J.F., Wong, G.T.F., Casey, W.H., 1985. Atmospheric fluxes and marsh-soil inventories of ^{7}Be and ^{210}Pb. J. Geophys. Res. 90 (D6), 10487–10495.

Ortt, R.A., Kerhin, R.T., Wells, D., Cornwell, J., 2000. Bathymetric survey and sedimentation analysis of Loch Raven and Prettyboy reservoirs. Coastal and Estuarine Geology File Report (99-4).

Palinkas, C., Nittrouer, C., Wheatcroft, R., Langone, L., 2005. The use of ^{7}Be to identify event and seasonal sedimentation near the Po River delta, Adriatic Sea. Mar. Geol. 222, 95–112.

Periáñez, R., Abril, J.M., 2014. A numerical modeling study on oceanographic conditions in the former Gulf of Tartessos (SW Iberia): tides and tsunami propagation. J. Mar. Syst. 139, 68–78.

Pfitzner, J., Brunskill, G., Zagorskis, I., 2004. ^{137}Cs and excess ^{210}Pb deposition patterns in estuarine and marine sediment in the central region of the Great Barrier Reef Lagoon, north-eastern Australia. J. Environ. Radioact. 76 (1), 81–102.

Pham, M.K., Povinec, P.P., Nies, H., Betti, M., 2013. Dry and wet deposition of ^{7}Be, ^{210}Pb and ^{137}Cs in Monaco air during 1998–2010: seasonal variations of deposition fluxes. J. Environ. Radioact. 120, 45–57.

Qu, W., Kelderman, P., 2001. Heavy metal contents in the Delft canal sediments and suspended solids of the River Rhine: multivariate analysis for source tracing. Chemosphere 45 (6), 919–925.

Robbins, J.A., 1978. Geochemical and geophysical applications of radioactive lead isotopes. In: Nriagu, J.O. (Ed.), Biogeochemistry of Lead. Elsevier.

Robbins, J.A., Holmes, C., Halley, R., Bothner, M., Shinn, E., Graney, J., Keeler, G., ten Brink, M., Orlandini, K.A., Rudnick, D., 2000. Time-averaged fluxes of lead and fallout radionuclides to sediments in Florida Bay. J. Geophys. Res. 105 (C12), 28805–28821.

Rose, L.E., Kuehl, S.A., 2010. 2010. Recent sedimentation patterns and facies distribution on the Poverty Shelf, New Zealand. Mar. Geol. 270, 160–174.

Schipper, C., Rietjens, I., Burgess, R., Murk, A., 2010. Application of bioassays in toxicological hazard, risk and impact assessments of dredged sediments. Mar. Pollut. Bull. 60 (11), 2026–2042.

Schmidt, S., Gonzalez, J.-L., Lecroart, P., Tronczyński, J., Billy, I., Jouanneau, J.-M., 2007a. Bioturbation at the water-sediment interface of the Thau Lagoon: impact of shellfish farming. Aquat. Living Resour. 20 (2), 163–169.

Schmidt, S., Jouanneau, J.-M., Weber, O., Lecroart, P., Radakovitch, O., Gilbert, F., Jézéquel, D., 2007b. Sedimentary processes in the Thau Lagoon (France): from seasonal to century time scales. Estuar. Coast. Shelf Sci. 72 (3), 534–542.

Sharma, P., Gardner, L., Moore, W., Bollinger, A., 1987. Sedimentation and bioturbation in a salt marsh as revealed by ^{210}Pb, ^{137}Cs, and ^{7}Be studies. Limnol. Oceanogr. 32 (2), 313–326.

Smith, J.N., 2001. Why should we believe 210 Pb sediment geochronologies? J. Environ. Radioact. 55 (2), 121–123.

Smith, J., Lee, K., Gobeil, C., Macdonald, R., 2009. Natural rates of sediment containment of PAH, PCB and metal inventories in Sydney Harbour, Nova Scotia. Sci. Total Environ. 407 (17), 4858–4869.

Sommerfield, C.K., Nittrouer, C.A., Alexander, C.R., 1999. ^{7}Be as a tracer of flood sedimentation on the northern California continental margin. Cont. Shelf Res. 19, 335–361.

Syvitski, J.P., Vörösmarty, C.J., Kettner, A.J., Green, P., 2005. Impact of humans on the flux of terrestrial sediment to the global coastal ocean. Science 308 (5720), 376–380.

Tang, CW.-y., Ip, CC.-m., Zhang, G., Shin, P.K., Qian, P.-y., Li, X.-d., 2008. The spatial and temporal distribution of heavy metals in sediments of Victoria Harbour, Hong Kong. Mar. Pollut. Bull. 57 (6), 816–825.

Tanner, P.A., Leong, L.S., Pan, S.M., 2000. Contamination of heavy metals in marine sediment cores from Victoria Harbour, Hong Kong. Mar. Pollut. Bull. 40 (9), 769–779.

Taylor, A., Blake, W.H., Smith, H.G., Mabit, L., Keith-Roach, M.J., 2013. Assumptions and challenges in the use of fallout beryllium-7 as a soil and sediment tracer in river basins. Earth Sci. Rev. 126, 85–95.

Thomas, S., Ridd, P., 2014. Review of methods to measure short time scale sediment accumulation. Mar. Geol. 207, 95–114.

Van Rijn, L.C., 2005. Estuarine and coastal sedimentation problems. Int. J. Sediment Res. 20 (1), 39–51.

de Vicente, I., Cruz-Pizarro, L., Rueda, F.J., 2010. Sediment resuspension in two adjacent shallow coastal lakes: controlling factors and consequences on phosphate dynamics. Aquat. Sci. 72 (1), 21–31.

Yeager, K., Santschi, P., Phillips, J., Herbert, B., 2005. Suspended sediment sources and tributary effects in the lower reaches of a coastal plain stream as indicated by radionuclides, Loco Bayou, Texas. Environ. Geol. 47 (3), 382–395.

Yusoff, A.H., Zulkifli, S.Z., Ismail, A., Mohamed, C.A.R., 2015. Vertical trend of trace metals deposition in sediment core off Tanjung Pelepas Harbour, Malaysia. Procedia Environ Sci 30, 211–216.